*nanomaterials*

MDPI

*Article*

# Electrochemical Performance of Photovoltaic Cells Using HDA Capped-SnS Nanocrystal from bis (*N*-1,4-Phenyl-*N*-Morpho-Dithiocarbamato) Sn(II) Complexes

**Johannes Z. Mbese [1,*], Edson L. Meyer [2,*] and Mojeed A. Agoro [1,2,*]**

[1] Department of Chemistry, University of Fort Hare, Private Bag X1314, Alice 5700, South Africa
[2] Fort Hare Institute of Technology, University of Fort Hare, Private Bag X1314, Alice 5700, South Africa
* Correspondence: jmbese@ufh.ac.za (J.Z.M.); emeyer@ufh.ac.za (E.L.M); magoro@ufh.ac.za (M.A.A.)

Received: 15 January 2020; Accepted: 19 February 2020; Published: 27 February 2020


**Abstract:** Great consideration is placed on the choice of capping agents' base on the proposed application, in order to cater to the particular surface, size, geometry, and functional group. Change in any of the above can influence the characteristics properties of the nanomaterials. The adoption of hexadecylamine (HDA) as a capping agent in single source precursor approach offers better quantum dots (QDs) sensitizer materials with good quantum efficiency photoluminescence and desirable particles size. Structural, morphological, and electrochemical instruments were used to evaluate the characterization and efficiency of the sensitizers. The cyclic voltammetry (CV) results display both reduction and oxidation peaks for both materials. XRD for SnS/HDA and SnS photosensitizers displays eleven peaks within the values of 27.02° to 66.05° for SnS/HDA and 26.03° to 66.04° for SnS in correlation to the orthorhombic structure. Current density–voltage (I–V) results for SnS/HDA exhibited a better performance compared to SnS sensitizers. Bode plot results indicate electrons lifetime (τ) for SnS/HDA photosensitizer have superiority to the SnS photosensitizer. The results connote that SnS/HDA exhibited a better performance compared to SnS sensitizers due to the presence of HDA capping agent.

**Keywords:** single-source precursor; quantum dots; semiconductors; electrochemical; photovoltaic cells

## 1. Introduction

Quantum dots sensitized solar cells (QDSSCs) are emerging innovations for photovoltaic cells as a replacement for the ideal dye-sensitized solar cells (DSSCs). The maximum efficiency of 13.4% obtained from inorganic sensitizer [1] has led many scientists to the research on fabricating better photosensitizes. That can portray a good generation of multiple excitons [2,3], panchromatic characteristics [4], and photostability [5] that will deal with the shortfall of molecular dyes in the traditional DSSCs. The fabrication of quantum dots (QDs) sensitizer materials to enhance this kind of solar cells has gained ground due to their diversity [6,7], tunable band-gap, cost-friendliness, and easy fabrication. QDs size can be controlled to obtain optimum band gap, as well as incorporate other semiconductor QDs materials as co-sensitized to enhance their photospectral properties and increase the conversion efficiency of QDSSCs (as seen in Figure 1) [8–10]. Moreover, the challenges involving metal-oxide surface and the absorbers poor contact due to the inabilities of photoinduced charge separation to directly penetrate each other served as a major restriction [11].

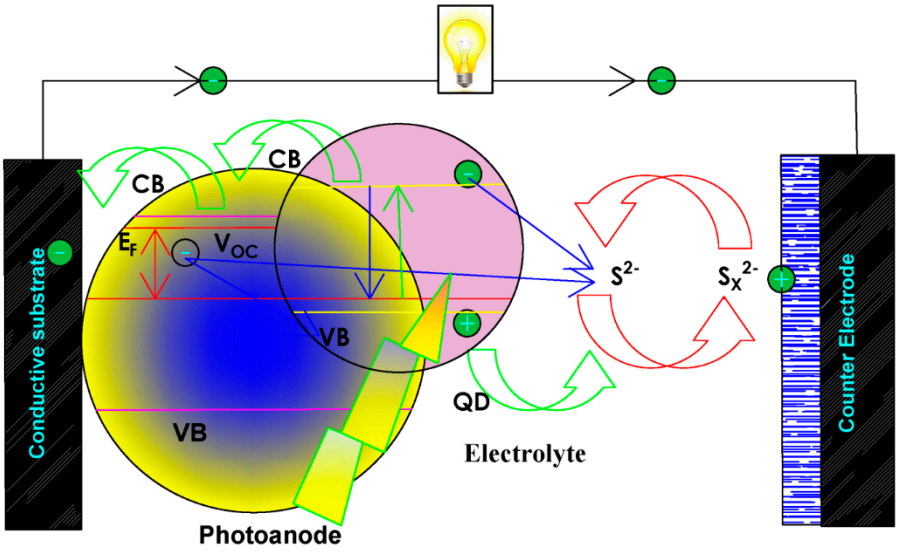


**Figure 1.** Schematic illustration of quantum dot solar cells (QDSCs) working procedure involving, quantum dots (QDs) photosensitizer, counter electrode, photoanode, and electrolyte [12].

Other limitation like electrons diffusion length and the electrode nanoporous oxide geometry [12], hinder the surface area optimum adsorption capacity of molecule dye. To increase the cell spectral properties by adopting various photosensitizers will lead to poor optical density [13]. This implies that the amount of solar radiation absorbed by the cells are linked directly to the nanoporous surface area of the electrodes. To solve this shortfall, nanoporous oxide can be separated from absorbers by injection of electrons to improve better overlap with the solar spectrum and higher optical density without destroying the electron absorption performance [14–16].

This can be achieved with synthetic process, which is divided into nucleation and growth. The depth knowledge about both steps has resulted in new nanosynthesis route. Giving a better uniform surface morphology, size and monodispersity materials by enabling optimum control on the synthesis process. Factors, such as solvent, reducing agent, and capping agent, are of very great importance in monodisperse nanoparticles synthesis. The use of capping agents in stabilization and colloidal synthesis of nanoparticles is known to control materials size, surface passivation and particle morphology. The adoption of energy-saving and less or non-toxic capping agents will promote green synthetic route of nanoparticle fabrication of large scale commercialization [17–19]. Great consideration is placed on the choice of capping agents' base on the proposed application, in other to cater for the particular surface, size, geometry and functional group. Change in any of the above mention can influence the characteristics properties of the materials. Capping agents, such as trioctylphophine oxide (TOPO), trioctylphophine (TOP), and hexadecylamine (HDA), etc., offer excellent stability with organic solvents for nanoparticles [20,21]. The injection of HDA capping agent could offer desirable particles size and better QDs sensitizer materials with good quantum efficiency. Therefore, enhancing the assembly patterns of the fabricated cells [22]. In the present study, the main objective is exploring the beneficial effects of both HDA capped and uncapped materials on surface treatments. Therefore, leading to improving electrochemical performance of quantum dots sensitizers' absorber in photovoltaic cells.

## 2. Materials and Methods

### *2.1. Material*

All materials were purchased and used without modification. The complete test kits containing fluorine-doped tin oxide (FTO) as glass substrate of $TiO_2$, platinum FTO, HI-30 electrolyte iodide, masks, gaskets, chenodeoxycholic acid (CDC) and hot seal were purchased from Solaronix Company

(Aubonne, Switzerland). Water, Oleic acid (OA), methanol, HDA, SnS/had, and SnS nanoparticles from bis (*N*-1,4-Phenyl-*N*-Morhpo-dithiocarbamato) Sn(II) complexes.

### 2.2. Synthesis of SnS Nanoparticles with HDA Capping Agent

Nanoparticles were fabricated according to the literature method [23] 0.20 g of bis (*N*-1,4-Phenyl-*N*-Morhpo-dithiocarbamato) tin(II) complex (as seen in Figure 2), was added to 4 mL oleic acid (OA) and were injected into hot HDA of 3 g at 360 °C for surface passivation and particle morphology. 20–30 °C initial temperature was attained for the mixture. The reaction was stabilized at 360 °C and the process lasted for 1 h. The process was allowed to drop to 70 °C signifying the completion of the process and about 50 mL methanol were used the remover of excess OA and HDA. Centrifugation was used to separate the flocculent precipitate and re-dispersed with toluene. Low air pressure was used to remove solvent giving rise to metals sulfides of SnS/HDA nanoparticles.

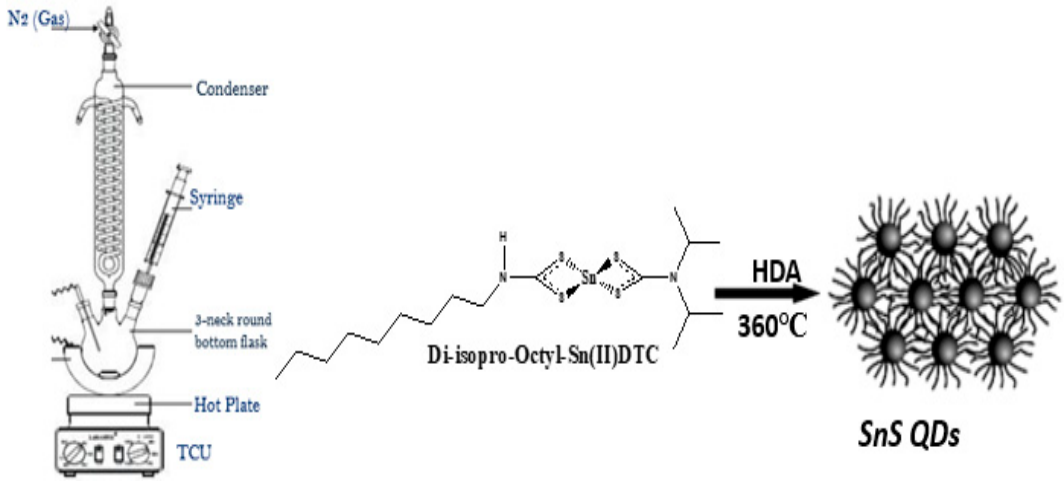


**Figure 2.** Schematic reaction of nanoparticles.

### 2.3. Synthesis of SnS Nanoparticles Without HDA Capping Agent

Synthesis of SnS nanocrystals was obtained through high-temperature thermal decomposition of bis (*N*-1,4-Phenyl-*N*-Morhpo-dithiocarbamato) tin(II) complex using Perkin Elmer TGA 4000 ThermoGravimetric Analyser (TGA) (San Jose, CA, USA). About 25 mg of the complex was loaded into an alumina pan and weight changes were recorded as a function of temperature for a 10 °C $min^{-1}$ temperature gradient between 30–900 °C. A purge gas of flowing nitrogen at a rate of 20 mL $min^{-1}$ was used. At temperatures between 360 and 900 °C, the complex end product was converted into residue, which was expected for the formation of SnS nanocrystals from the residue obtained from the TGA.

### 2.4. Fabrication and Assembling of Solar Cells

QDSSC were prepared with 2 × 2 $cm^2$ FTO-glass plates of platinum and $TiO_2$ electrodes were purchase from Solaronix (Aubonne, Switzerland) with 6 × 6 $mm^p$ active areas of $TiO_2$ screen coated. Dye loading for sensitization was done using 10 mL of warm water with MO-SnS/HDA and MO-SnS. Co-adsorbents were added (Co-adsorbent/dye) of chenodeoxycholic acid (CDC) were used. The mediating solution was the commercial HI-30 electrolyte solution (Solaronix), with content of iodide species at 0.05 M. The $TiO_2$ thin film was soaked into a solution of photosensitizers for 24 h. The two substrates, one coated with $TiO_2$ loaded with photosensitizers and the other with platinum, were held together using polyethylene and soldering iron. The syringe was used to inject the HI-30 electrolyte (iodide).

Characterization and solar cell conversion efficiency (%) measurements were done using Equations (1)–(4) mentioned below.

All substitutions would be done following Equations (1)–(4).

$$Jsc = (Isc\ (mA))/(A(cm^2)) \quad (1)$$

$$FF = (V_{MAX} \times J_{MAX})/(V_{OC} \times J_{SC}) \quad (2)$$

Where FF is fill factor, and $V_{OC}$ is an open circuit voltage; $J_{SC}$ is a short circuit current density.

$$\eta\ (\%) = (V_{MAX} \times J_{MAX})/P\mathit{in}. \quad (3)$$

The above equation was adopted where P*in* is a light intensity of 100 mW $cm^{-2}$.

$$\eta\ (\%) = (V_{OC} \times J_{SC} \times FF)/P\mathit{in} \times 100\%. \quad (4)$$

The final equation for overall conversion efficiency was derived from the following equation.

### *2.5. Physical Measurements*

Electrochemical studies were carried out using Metrohm 85695 Autolab with Nova 1.10 software (Metrohm South Africa (Pty) Ltd., Sandton, South Africa). A platinum electrode was adopted as a counter electrode, with $TiO_2$ as the anode, while HI-30 iodode electrode was used as a reference electrode. Cyclic voltammetry (CV) was performed at scan rates from 0.05 to 0.35 V $s^{-1}$ with an increment of 0.05 V $s^{-1}$. All the experiments were performed at room temperature. Electrochemical impedance spectroscopy (EIS) was carried out in the frequency range of 100 kHz to 100 mHz. Current density–voltage (I–V) parameters were collected through a Keithley 2401 source meter and a Thorax light power meter. Lumixo AM1.5 light simulator (RS Components (SA), Midrand, South Africa) was employed, and the lamp was fixed at 50 cm high to avoid illumination outside of the working area. To avoid cells degradation, temperature was kept below 60 °C and the light power density at 100 mW $cm^{-2}$ (AM1.0). X-ray diffractometer (XRD) were employed to evaluate the structural pattern of the samples, and the diffraction structure was obtained between 10 and 90° at the interval of 0.05°. The surface roughness of the SnS/HDA and SnS FTO substrates were identified through the use of atomic force microscopy (AFM) (JPK NanoWizard II AFM, JPK Instruments, Berlin, Germany) at a scan rate of 0.8 Hz in contact mode. JEOL JEM 2100 High-Resolution Transmission Electron Microscope (JEOL Inc., Pleasanton, CA, USA) (HRTEM) operating at 200 KV with selected area electron diffraction (SAED) patterns was used.

## 3. Results and Discussion

SnS/HDA and SnS sensitizers were employed to investigate the optimized electrochemical performance of both materials. Figure 3 shows comparative CV curves of two the materials at fix applied amplitude of 50 mV $s^{-1}$. The measurement shows precise redox peaks at the voltage of 0.0 and 0.6 V, confirming the charge storage by redox reactions. The kinetic irreversibility of both displaced materials has asymmetry, i.e., reduction and oxidation of the CV curves [24,25]. SnS sensitizer exhibited a higher area than SnS/HDA, which is preferred for higher performance abilities.

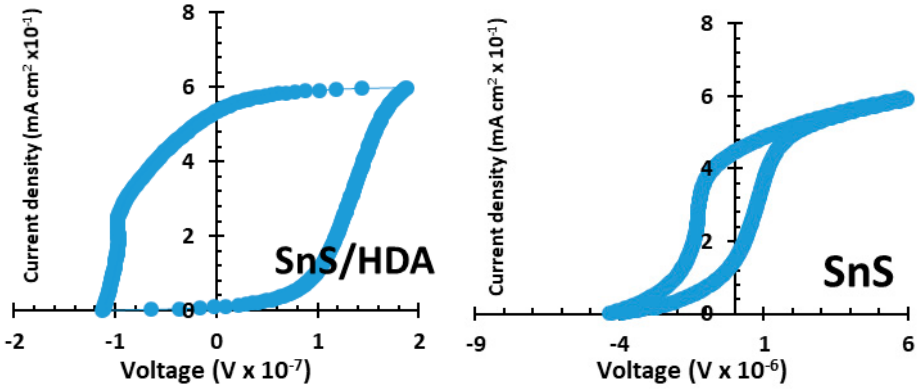


**Figure 3.** Cyclic voltammetry (CV) spectra of SnS/HDA and SnS nanoparticles.

Based on the EIS results of SnS/HDA and SnS photosensitizer, shown in Figure 4, the charge transfer resistance ($R_{ct}$) of the SnS sensitizer film decreases compare to the SnS/HDA sensitizer with lower charge transfer resistivity. These will enhance fast electron transfer, lower charge recombination, and better conductivity compared to SnS/HDA photosensitizer. This connotes improved contact between the redox couple with SnS sensitizer and a better degree of electron growth [26,27]. By this, we concluded that SnS sensitizer offers preferable efficient electron transfer.

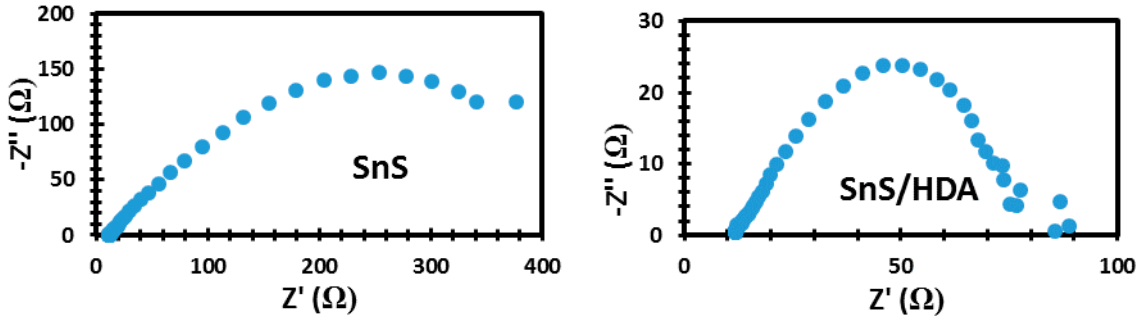


**Figure 4.** Electrochemical impedance spectroscopy (EIS) spectra of SnS/HDA and SnS nanoparticles.

The appropriate instrument to investigate structural phase unit cell dimension and lattice parameters of SnS/HDA and SnS photosensitizer films is X-ray diffraction (XRD) analysis. Figure 5 reveals the XRD configurations. Their peaks of 2$\theta$ range between 27–82° that correlated to orthorhombic SnS crystals (JCPDS 039-0354). Furthermore, both materials display no traces of other impurities as observed in the XRD patterns. The purity and quality of the crystalline are displayed by the strong and sharp diffraction peaks observed in both samples. The improvement in crystalline quality could be linked to nucleation control, which promotes the growth process of SnS [28]. In addition, there is no change in the preferential orientation along (201), (210), (111), (301), (311), (511), (610), and (512) for both samples, which confirms successful fabrication of SnS and SnS/HDA into the lattice of $TiO_2$ [29]. The preferential orientation of SnS/HDA is linked to the nucleation control of the growth process due to excess HDA used during the synthesis [30]. The presence of lower intensities and minor phases are usually linked to defect chemistry, thermodynamics of solid, and thermal gradient.

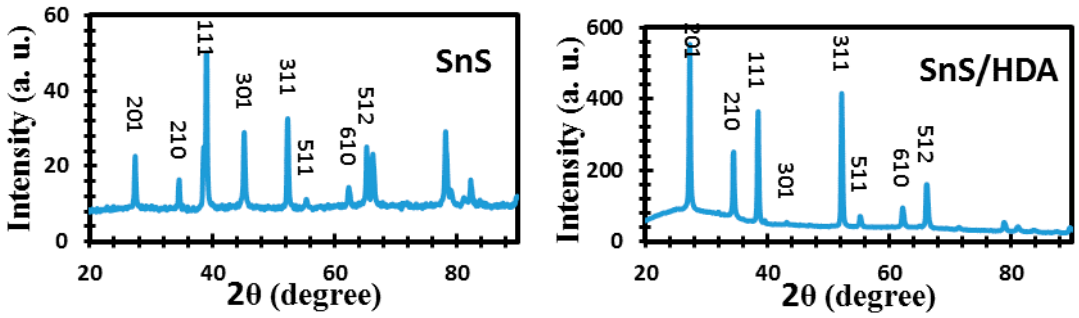


**Figure 5.** XRD spectra of SnS/HDA and SnS nanoparticles.

Table 1 and Figure 6 display I–V parameters of SnS/HDA and SnS photosensitizers quantum dot solar cells (QDSCs). $TiO_2$ photoanode sensitized with the fabricated dye, and Pt counter electrode and redox couple HI-30 electrolyte was used. In order to evaluate the efficiency of the photosensitized materials, these materials were fabricated with the same test conditions. The SnS/HDA and SnS JSC is observed at 10.99 mA $cm^{-2}$ and 1.802 mA $cm^{-2}$, producing conversion efficiency at 1.25% and 0.42%. Their photovoltaic characteristics of QDSSCs films based for $V_{OC}$ are 0.423 V and 0.375 V. The lower conversion efficiency of SnS compared to SnS/HDA could be linked to the low electrocatalytic activity, which reduce HI-30 iodide and low electrical conductivity. These hinder electron transport from recombining with holes because of redox couple [31].

**Table 1.** I–V characteristics of SnS/HDA and SnS nanoparticles.

| Dye | Photoanode | Electrolyte | CEs | $J_{SC}$ (mA/cm$^2$) | $V_{OC}$ (mV) | FF | η (%) |
|---|---|---|---|---|---|---|---|
| **SnS/HDA** | $TiO_2$ | HI-30 | Pt | 10.99 | 0.423 | 0.27 | **1.25** |
| **SnS** | $TiO_2$ | HI-30 | Pt | 1.802 | 0.375 | 0.63 | **0.42** |

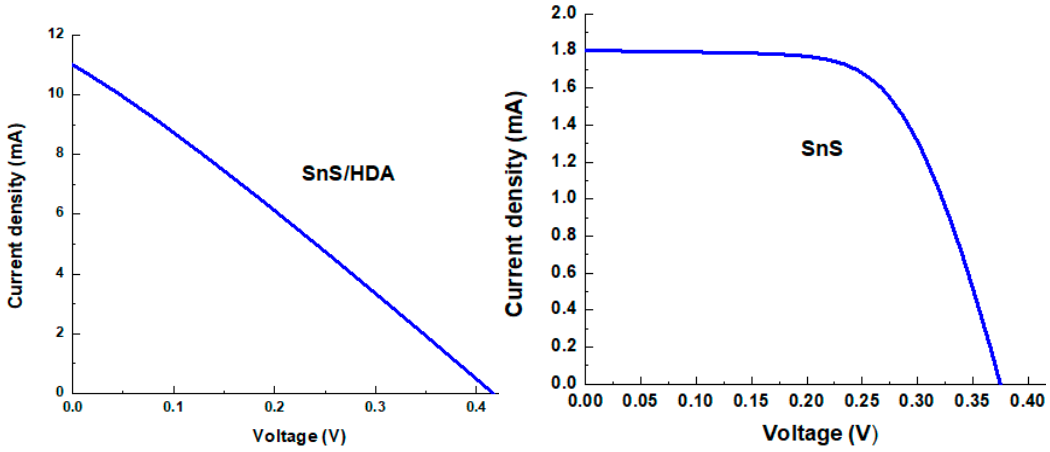


**Figure 6.** I–V curve characteristics of SnS/HDA and SnS nanoparticles.

The Bode plot, as seen in Figure 7, exhibits the phase angle shift and frequency response magnitude. According to Bode plot, the phase angle of SnS photosensitizer is higher compared to SnS/HDA photosensitizer. This depicts that SnS has a porous nature (confirmed by surface area analysis and AFM image) and lower charge transfer resistance. Furthermore, this enhances the injection and flow of electrolyte in the cell [32].

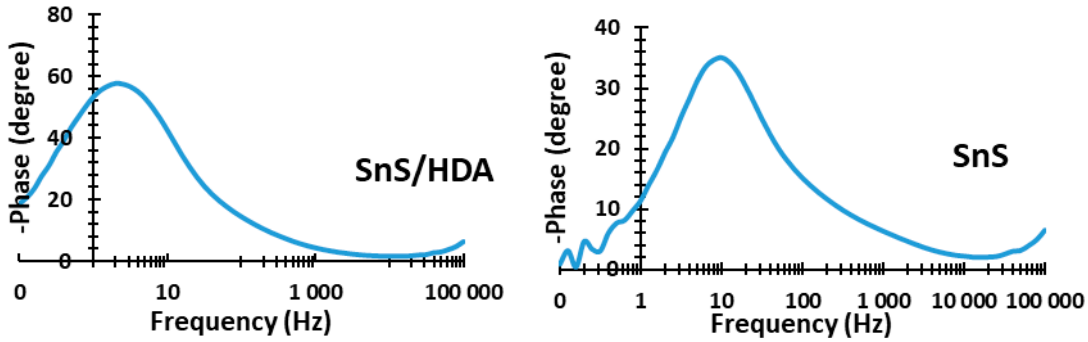


**Figure 7.** Bode plot spectra of SnS/HDA and SnS nanoparticles.

The topographical analysis was carried out using atomic force microscope (AFM). The evaluated particles size varied in the range of 0.11–1.18 um for SnS/HDA and 0.054–0.54 um for SnS films grown at 360 °C with size height of 16.8% and 8.4%, respectively, as seen in Figure 8. These images revealed little significant changes in the particles size of both samples fabricated at the same temperature. The ad-atoms move over the surface brings bonding togetherness with an enlarged form of sub-particles. This emanated to formation good compactness and larger particles size. When the film surface is smooth, it resulted to lower roughness due to high surface diffusion [33]. This can be attributed to better particle size and good power conversion efficiency in QDSSCs, which depends solely on the low roughness of the photoelectrodes.

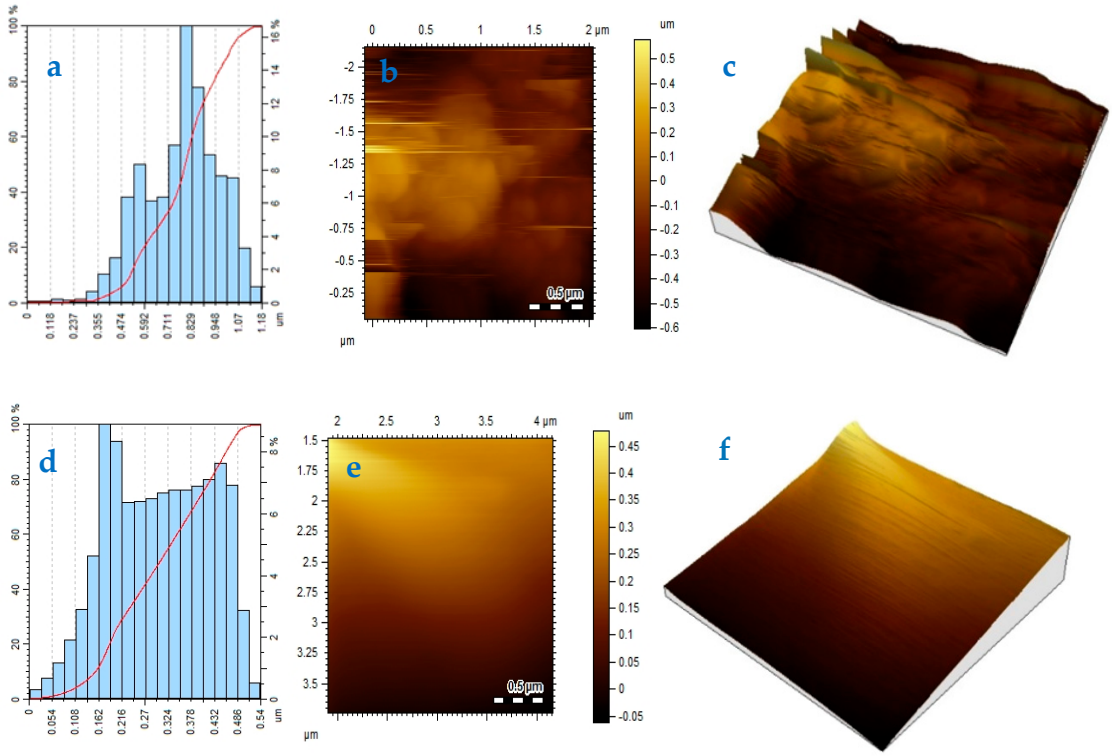


**Figure 8.** Height profile (**a**,**d**), 2D (**b**,**e**), and 3D (**c**) atomic force microscopy (AFM) images of SnS (**a**–**c**) and SnS/HDA (**d**–**f**) nanoparticles.

The measurements and morphology of the synthesized SnS/HDA and SnS were examined by HRTEM; Figure 9 reveals, that the products are spherical, clustered, and agglomerated, with crystallite sizes within the range 14.96–44.39 nm for SnS and 9.5–23.19 nm for SnS/HDA [34]. Their lattice fringes revealed polycrystalline nanoparticles comprising numerous crystal grains d-spacing of 3.549–3.623 nm, affirming their polycrystalline nature, which is in concurrence with the report from Reference [35].

SAED obtained reveals the spot pattern shaping of the diffraction rings, which indicates that both materials have high crystalline nature [36].

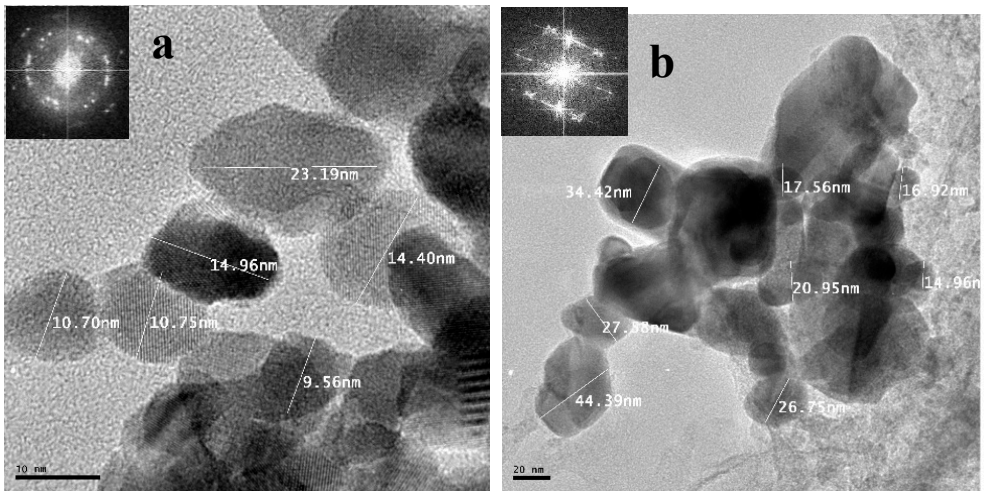


**Figure 9.** High-Resolution Transmission Electron Microscope (HRTEM) images of (**a**) SnS/HDA and (**b**) SnS nanoparticles.

## 4. Conclusions

In the CV curve of SnS/HDA and SnS sensitizers, the spectra displaced both reduction and oxidation peaks for both materials. The diffusion of SnS/HDA and SnS photosensitizer in HI-30 electrolyte connote Warburg's constant (W) as a result of the straight line. The SnS/HDA sensitizer displaced lower impedance compare to SnS sensitizer. XRD results for SnS/HDA and SnS photosensitizers displaced eleven peaks within the values of 27.02° to 66.05° for SnS/HDA and 26.03° to 66.04° for SnS in correlation to orthorhombic structure. The I–V efficiency obtained indicates that the SnS/HDA exhibited a better performance compared to SnS and Sn(II) sensitizers due to the presence of HDA capping agent. Bode plot results indicate that the electrons lifetime ($\tau$) for SnS/HDA photosensitizer displaced superiority to the SnS photosensitizer, owning to their ability to enhanced electron lifetime and reduced electron recombination. The AFM results show the particle size distribution in SnS value at 357 nm with a smooth surface and good compactness on the substrate. However, the value for SnS/HDA is 122 nm displaced shape and size of non-symmetrical particles. The lattice fringes revealed polycrystalline nanoparticles comprising numerous crystal grains for both samples.

**Author Contributions:** Conceptualization, J.Z.M., M.A.A. and E.L.M.; methodology, J.Z.M., M.A.A. and E.L.M.; validation, J.Z.M., M.A.A. and E.L.M.; formal analysis, J.Z.M., M.A.A, and E.L.M.; investigation, M.A.A.; resources, J.Z.M., M.A.A. and E.L.M.; data curation, J.Z.M., M.A.A. and E.L.M.; writing—original draft preparation M.A.A.; writing—review and editing M.A.A.; visualization, M.A.A.; supervision, J.Z.M. and E.L.M.; funding acquisition, J.Z.M. and E.L.M. All authors have read and agreed to the published version of the manuscript.

**Funding:** The authors wish to acknowledge the National Department of Science and Technology (GUN: 86187) of South Africa and its implementing agent, the National Research Foundation (GUN: 93215) for the financial support. Authors are also grateful for the financial support by Govan Mbeki Research and Development Centre (GMRDC), University of Fort Hare, South Africa and NRF Thuthuka Grant (GUN: 118139); Eskom TESP (P948).

**Acknowledgments:** The authors appreciate the support from K.M. (Kbizz IT support) for the visualization of data and to the Inorganic, Energy and Material Research Group (IEMRG) at the university of Fort Hare for allowing to use their laboratory, materials and instruments.

**Conflicts of Interest:** The authors declare no conflict of interest.

## References


1. Mathew, S.; Yella, A.; Gao, P.; Humphry-Baker, R.; Curchod, B.F.E.; Astani, N.A.; Tavernelli, I.; Rothlisberger, U.; Nazeeruddin, K.; Grätzel, M. Dye-sensitized solar cells with 13% efficiency achieved through the molecular engineering of porphyrin sensitizers. *Nat. Chem.* **2014**, *6*, 242–247. [CrossRef] [PubMed]
2. Seol, M.; Ramasamy, E.; Lee, J.; Yong, K. Highly Efficient and Durable Quantum Dot Sensitized ZnO Nanowire Solar Cell Using Noble-Metal-Free Counter Electrode. *J. Phys. Chem. C* **2011**, *115*, 22018–22024. [CrossRef]
3. Santra, P.; Kamat, P. Tandem-Layered Quantum Dot Solar Cells: Tuning the Photovoltaic Response with Luminescent Ternary Cadmium Chalcogenides. *J. Am. Chem. Soc.* **2013**, *135*, 877–885. [CrossRef] [PubMed]
4. Beard, M.C. Multiple Exciton Generation in Semiconductor Quantum Dots. *J. Phys. Chem. Lett.* **2011**, *2*, 1282–1288. [CrossRef]
5. Semonin, O.E.; Luther, J.M.; Choi, S.; Chen, H.-Y.; Gao, J.; Nozik, A.J.; Beard, M.C. Peak External Photocurrent Quantum Efficiency Exceeding 100% via MEG in a Quantum Dot Solar Cell. *Science* **2011**, *334*, 1530–1533. [CrossRef]
6. Shu, T.; Zhou, Z.; Wang, H.; Liu, G.; Xiang, P.; Rong, Y.; Han, H.; Zhao, Y. Efficient quantum dot-sensitized solar cell with tunable energy band CdSe × S (1 − x) quantum dots. *J. Mater. Chem.* **2012**, *22*, 10525–10529. [CrossRef]
7. Dey, P.; Paul, J.; Bylsma, J.; Karaiskaj, D.; Luther, J.M.; Beard, M.C.; Romero, A. Origin of the temperature dependence of the band gap of PbS and PbSe quantum dots. *Solid State Commun.* **2013**, *165*, 49–54. [CrossRef]
8. Sargent, E.H. Colloidal quantum dot solar cells. *Nat. Photonics* **2012**, *6*, 133–135. [CrossRef]
9. Gimenez, S.; Mora-Seró, I.; Macor, L.; Guijarro, N.; Lana-Villarreal, T.; Gómez, R.; Diguna, L.J.; Shen, Q.; Toyoda, T.; Bisquert, J. Improving the performance of colloidal quantum-dot-sensitized solar cells. *Nanotechnology* **2009**, *20*, 295204. [CrossRef]
10. Abbas, M.A.; Basit, M.A.; Park, T.J.; Bang, J.H. Enhanced performance of PbS-sensitized solar cells via controlled successive ionic-layer adsorption and reaction. *Phys. Chem. Chem. Phys.* **2015**, *17*, 9752–9760. [CrossRef]
11. Grätzel, M. Dye-sensitized solar cells. *J. Photochem. Photobiol. C Photochem. Rev.* **2003**, *4*, 145–153. [CrossRef]
12. Meyer, E.L.; Mbese, J.Z.; Agoro, M.A. The Frontiers of Nanomaterials (SnS, PbS and CuS) for Dye-Sensitized Solar Cell Applications: An Exciting New Infrared Material. *Molecules* **2019**, *24*, 4223. [CrossRef] [PubMed]
13. Lee, H.; Leventis, H.C.; Moon, S.-J.; Chen, P.; Ito, S.; Haque, S.A.; Torres, T.; Nüesch, F.; Geiger, T.; Zakeeruddin, S.M.; et al. PbS and CdS Quantum Dot-Sensitized Solid-State Solar Cells: "Old Concepts, New Results". *Adv. Funct. Mater.* **2009**, *19*, 2735–2742. [CrossRef]
14. Hardin, B.E.; Hoke, E.T.; Armstrong, P.B.; Yum, J.H.; Comte, P.; Torres, T.; Fréchet, J.M.; Nazeeruddin, M.K.; Grätzel, M.; McGehee, M.D. Increased light harvesting in dye-sensitized solar cells with energy relay dyes. *Nat. Photonics* **2009**, *3*, 406. [CrossRef]
15. Shankar, K.; Feng, X.; Grimes, C.A. Enhanced Harvesting of Red Photons in Nanowire Solar Cells: Evidence of Resonance Energy Transfer. *ACS Nano* **2009**, *3*, 788–794. [CrossRef]
16. Shalom, M.; Albero, J.; Tachan, Z.; Martinez-Ferrero, E.; Zaban, A.; Palomares, E.J. Quantum Dot−Dye Bilayer-Sensitized Solar Cells: Breaking the Limits Imposed by the Low Absorbance of Dye Monolayers. *J. Phys. Chem. Lett.* **2010**, *1*, 1134–1138. [CrossRef]
17. Sun, Y.; Xia, Y. Shape-Controlled Synthesis of Gold and Silver Nanoparticles. *Science* **2002**, *298*, 2176–2179. [CrossRef]
18. Wang, D.; Peng, Q.; Li, Y. Nanocrystalline intermetallics and alloys. *Nano Res.* **2010**, *3*, 574–580. [CrossRef]
19. Duan, H.; Wang, D.; Li, Y. Green chemistry for nanoparticle synthesis. *Chem. Soc. Rev.* **2015**, *44*, 5778–5792. [CrossRef] [PubMed]
20. Soliwoda, K.; Tomaszewska, E.; Tkacz-Szczesna, B.; Mackiewicz, E.; Rosowski, M.; Bald, A.; Blanck, C.; Schmutz, M.; Novak, J.; Schreiber, F.; et al. Effect of the Alkyl Chain Length of Secondary Amines on the Phase Transfer of Gold Nanoparticles from Water to Toluene. *Langmuir* **2014**, *30*, 6684–6693. [CrossRef] [PubMed]
21. Barman, S.R.; Nain, A.; Jain, S.; Punjabi, N.; Mukherji, S.; Satija, J. Dendrimer as a multifunctional capping agent for metal nanoparticles for use in bioimaging, drug delivery and sensor applications. *J. Mater. Chem. B* **2018**, *6*, 2368–2384. [CrossRef]

22. Gulati, S.; Sachdeva, M.; Bhasin, K.K. Capping agents in nanoparticle synthesis: Surfactant and solvent system. *AIP Conf. Proc.* **2018**, *1953*, 030214.
23. Mbese, J.Z.; Ajibade, P.A.; Matebese, F.; Agoro, M.A. Optical and Structural Properties of TOPO/HDA Capped CuS Nanocrystals via Thermal Decomposition of Bis(N-Diisopropyldithiocarbamate)Cu(II) Complex. *J. Nano Res.* **2019**, *59*, 161–165. [CrossRef]
24. Meher, S.K.; Justin, P.; Rao, G.R. Nanoscale morphology dependent pseudocapacitance of NiO: Influence of intercalating anions during synthesis. *Nanoscale* **2011**, *3*, 683–692. [CrossRef]
25. Patil, A.; Lokhande, A.; Shinde, P.; Shelke, H.; Lokhande, C. Electrochemical supercapacitor properties of SnS thin films deposited by low-cost chemical bath deposition route. *Int. J. Eng.* **2017**, *10*, 914–922.
26. Wang, L.; Gu, X.; Zhao, Y.; Qiang, Y.; Huang, C.; Song, J. Preparation of ZnO/ZnS thin films for enhancing the photoelectrochemical performance of ZnO. *Vacuum* **2018**, *148*, 201–205. [CrossRef]
27. Kafashan, H. Optoelectronic properties of In-doped SnS thin films. *Ceram. Int.* **2019**, *45*, 334–345. [CrossRef]
28. Kafashan, H.; Azizieh, M.; Balak, Z. Electrochemical synthesis of nanostructured Se-doped SnS: Effect of Se-dopant on surface characterizations. *Appl. Surf. Sci.* **2017**, *410*, 186–195. [CrossRef]
29. Yang, Z.; Chen, C.-Y.; Liu, C.-W.; Chang, H.-T. Electrocatalytic sulfur electrodes for CdS/CdSe quantum dot-sensitized solar cells. *Chem. Commun.* **2010**, *46*, 5485. [CrossRef] [PubMed]
30. Meyer, E.L.; Mbese, J.Z.; Agoro, M.A.; Taziwa, R. Optical and structural-chemistry of SnS nanocrystals prepared by thermal decomposition of bis(N-di-isopropyl-N-octyl dithiocarbamato)tin(II) complex for promising materials in solar cell applications. *Opt. Quantum Electron.* **2020**, *52*, 90. [CrossRef]
31. Hou, Y.; Wang, N.; Yang, X.H.; Fang, W.Q.; Zhang, B.; Wang, H.F.; Lu, G.Z.; Hu, P.; Zhao, H.; Yang, H.G. Rational screening low-cost counter electrodes for dye-sensitized solar cells. *Nat. Commun.* **2013**, *4*, 1583. [CrossRef] [PubMed]
32. Chen, J.-G.; Wei, H.-Y.; Ho, K.-C. Using modified poly(3,4-ethylene dioxythiophene): Poly(styrene sulfonate) film as a counter electrode in dye-sensitized solar cells. *Sol. Energy Mater. Sol. Cells* **2007**, *91*, 1472–1477. [CrossRef]
33. Reddy, V.R.M.; Gedi, S.; Park, C.; Miles, R.W.; Reddy, K.T.R. Development of sulphurized SnS thin film solar cells. *Curr. Appl. Phys.* **2015**, *15*, 588–598. [CrossRef]
34. Pan, J.; Li, J.Y.; Xiong, S.L.; Qian, Y. Ultrasonically Assisted Synthesis of Tin Sulfide Nanorods at Room Temperature. *Adv. Mater. Res.* **2009**, *79*, 313–316. [CrossRef]
35. Jain, P.; Arun, P. Influence of grain size on the band-gap of annealed SnS thin films. *Thin Solid Films* **2013**, *548*, 241–246. [CrossRef]
36. Caskey, C.M.; Holder, A.; Shulda, S.; Christensen, S.T.; Diercks, D.; Schwartz, C.P.; Biagioni, D.; Nordlund, D.; Kukliansky, A.; Natan, A.; et al. Synthesis of a mixed-valent tin nitride and considerations of its possible crystal structures. *J. Chem. Phys.* **2016**, *144*, 144201. [CrossRef]